This is a repository copy of *2D Doppler backscattering using synthetic aperture microwave imaging of MAST edge plasmas*.

White Rose Research Online URL for this paper:
https://eprints.whiterose.ac.uk/94158/

Version: Published Version

Article:

2D Doppler backscattering using synthetic aperture microwave imaging of MAST edge plasmas

D.A. Thomas[1,2], K.J. Brunner[3], S.J. Freethy[1,2], B.K. Huang[2,3], V.F. Shevchenko[2] and R.G.L. Vann[1]

[1] York Plasma Institute, Department of Physics, University of York, York YO10 5DD, UK
[2] CCFE, Culham Science Centre, Abingdon, Oxon, OX14 3DB, UK
[3] Centre for Advanced Instrumentation (CfAI), Department of Physics, Durham University, Durham, DH1 3LE, UK

E-mail: dadt500@york.ac.uk

CrossMark

Abstract

Doppler backscattering (DBS) is already established as a powerful diagnostic; its extension to 2D enables imaging of turbulence characteristics from an extended region of the cut-off surface. The Synthetic Aperture Microwave Imaging (SAMI) diagnostic has conducted proof-of-principle 2D DBS experiments of MAST edge plasma. SAMI actively probes the plasma edge using a wide ($\pm40°$ vertical and horizontal) and tuneable (10–34.5 GHz) beam. The Doppler backscattered signal is digitised in vector form using an array of eight Vivaldi PCB antennas. This allows the receiving array to be focused in any direction within the field of view simultaneously to an angular range of 6–24° FWHM at 10–34.5 GHz. This capability is unique to SAMI and is a novel way of conducting DBS experiments. In this paper the feasibility of conducting 2D DBS experiments is explored. Initial observations of phenomena previously measured by conventional DBS experiments are presented; such as momentum injection from neutral beams and an abrupt change in power and turbulence velocity coinciding with the onset of H-mode. In addition, being able to carry out 2D DBS imaging allows a measurement of magnetic pitch angle to be made; preliminary results are presented. Capabilities gained through steering a beam using a phased array and the limitations of this technique are discussed.

Keywords: plasma diagnostics, doppler effect, reflectometry, density fluctuation, magnetic fields, scattering, antennas

(Some figures may appear in colour only in the online journal)

1. Introduction

Doppler backscattering (DBS), also called Doppler reflectometry, was developed from conventional reflectometry when fluctuations propagating perpendicular to the magnetic field were causing phase runaway while the antenna was oriented oblique to the cutoff surface [1]. DBS maintains many of the advantages of reflectometry including: infrequent access to the machine needed, only a small amount of port space required and high spatial and temporal resolution. As with most microwave diagnostics, DBS experiments can be conducted using antennas constructed from materials that are resistant to high heat and neutron flux environments. In addition, waveguides allow electronic components to be delocalised from the reactor and placed behind neutron shielding if necessary. Therefore, DBS is one of the few plasma diagnostic techniques that is
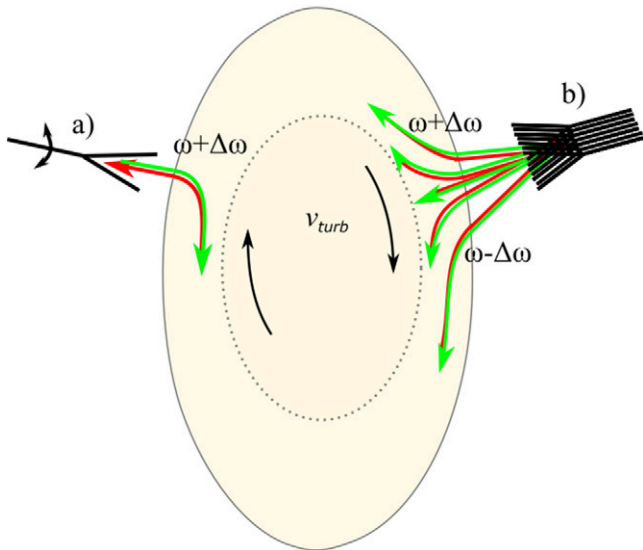
Figure 1. Poloidal cross-section cartoon of DBS. The plasma is indicated by the beige region. The incident probing beams are shown in green and the backscattered beams are shown in red. The direction of the turbulence velocity is indicated by the black arrows. The normal incidence O-mode cutoff is indicated by the dotted black line. (*a*) A steerable conventional single horn DBS experiment. (*b*) The SAMI diagnostic probes the the plasma with a broad beam and receives backscattered radiation from multiple directions and Doppler shifts using eight phase sensitive antennas.

suitable for deployment on next generation fusion devices; this renders its development crucial.

DBS experiments have been used to measure the perpendicular velocity profiles of turbulence structurures and turbulence amplitude at ASDEX Upgrade (AUG) [2], DIII-D [3], W7-AS [4, 5], EAST [6], HL-2A [7], LHD [8], L-2M [9] and MAST [10]. Turbulence velocity profiles are of interest as radial velocity shear has been shown to influence the stability properties of drift-type instabilities, for example [11]. Mechanically steerable mirrors and antennas have allowed k spectra to be measured in addition to turbulence velocity at DIII-D [12], TJ-II [13], Tore Supra [14] and AUG [15]. DBS has also been used to study the toroidal and radial structure of geodesic acoustic modes at DIII-D [3, 16, 17], AUG [18], TCV [19], Tore Supra [20] and FT-2 [21]. The perpendicular velocity, size and quasi-toroidal mode numbers of filaments in the edge region were determined using DBS at Globus-M [22].

A conventional DBS experiment comprises a horn antenna launching a beam oriented perpendicular to the magnetic field and *oblique* to the normal incidence cutoff surface (see figure 1(*a*)). The returned signal is Bragg-backscattered off turbulent structures elongated along the magnetic field lines. Due to refraction the backscattering occurs at a layer that is shifted radially outwards from the normal incidence cutoff. Backscattering occurs according to the Bragg condition near the cutoff

$$K_\perp \simeq -2k \qquad (1)$$

where $K_\perp$ is the *binormal* component of the density perturbations perpendicular to the equilibrium magnetic field and density surface normal. The incident wavenumber of the probing

beam *at the scattering location* is given by k. As the probing beam propagates through the plasma into regions of higher density k will decrease. Near the cutoff backscattering will occur continuously along the path of the beam. However, the amplitude of the turbulence decreases with wavenumber as K^{-3} or faster [23] and the scattering efficiency is $\propto K^{-2}$ [24]. In addition the electric field of the probing beam increases as the beam propagates towards higher density [24, 25]. These two effects highly localise backscattering to the region of lowest possible k. If the probing frequency is denoted by ω, and Doppler shift by $\Delta\omega$; $\Delta\omega$ is then linearly proportional to the perpendicular velocity of the density turbulence given by $v_{\text{turb}} = v_{E \times B} + v_{\text{phase}}$, where $v_{E \times B}$ is the plasma $E \times B$ velocity and v_{phase} is the phase velocity of the turbulent structures. In many cases [2, 4] the $E \times B$ flow dominates allowing the radial electric field, E_r, to be calculated using $E_r = -v_{E \times B}B$ [26].

In many conventional DBS experiments the back-scattered radiation is detected by a single horn antenna (figure 1(*a*)). In the linear regime the scattered power is proportional to the density fluctuation power [27] and the beam is Doppler shifted by the lab frame propagation velocity of the turbulent structures. In order to change viewing orientation, and therefore scattering wavenumber, a narrow beam is mechanically steered between shots [10]. In contrast, the Synthetic Aperture Microwave Imaging Diagnostic (SAMI) conducts DBS experiments by launching a broad ($\pm 40°$ horizontal and vertical) beam containing both O and X-mode polarisations using an antipodal Vivaldi PCB antenna [28, 29] and receives the backscattered signal on eight antenna channels simultaneously using an array of 8 Vivaldi antennas (figure 1(*b*)). The signals form each antenna are then downconverted and the phase and amplitude digitised. This allows the SAMI receiving beam to be focused in every direction simultaneously within $\pm 40°$, horizontal and vertical. This capability is unique to SAMI and is an entirely novel way of conducting DBS experiments.

2. Method

2.1. The SAMI diagnostic

In addition to SAMI, two DBS experiments have been conducted on spherical tokamak plasmas: one focusing on the edge [22], one focusing on the core [10]. Both of these experiments steered their probing beam mechanically.

SAMI uses an array of independently phased, linearly polarised antennas (see figure 3) where the receiving antennas are placed in order to minimise the side-lobe level in the reconstructed image. The array design was optimised using a simulated annealing global optimisation algorithm which is based on the analogy of annealing in metallurgy. The optimisation method is described further in [31] and [32].

SAMI acquires data at one RF frequency at a time and can switch between frequency channels with a switching time of 300 ns during the shot in any order (16 frequencies available 10, 11, 12, 13, 14, 15, 16, 17, 18, 20.5, 22.5, 24.5 26.5, 28.5, 30.5 and 34.5 GHz) primarily probing the edge region of the MAST plasma (see figure 2).
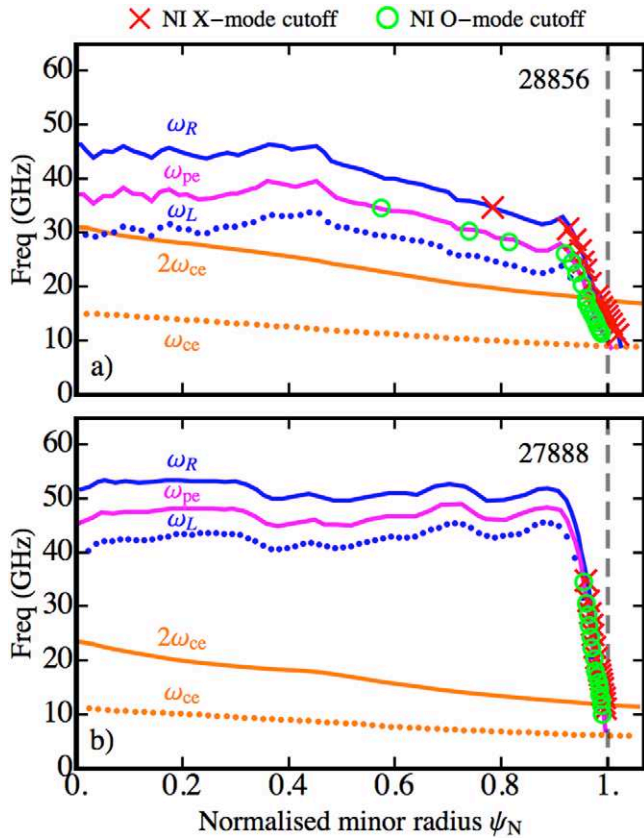
Figure 2. Normal incidence cutoffs for two MAST shots: (*a*) 28 856 in L-mode and (*b*) 27 888 in H-mode. Blue continuous and dotted lines indicate the normal incidence X-mode right-hand ($\om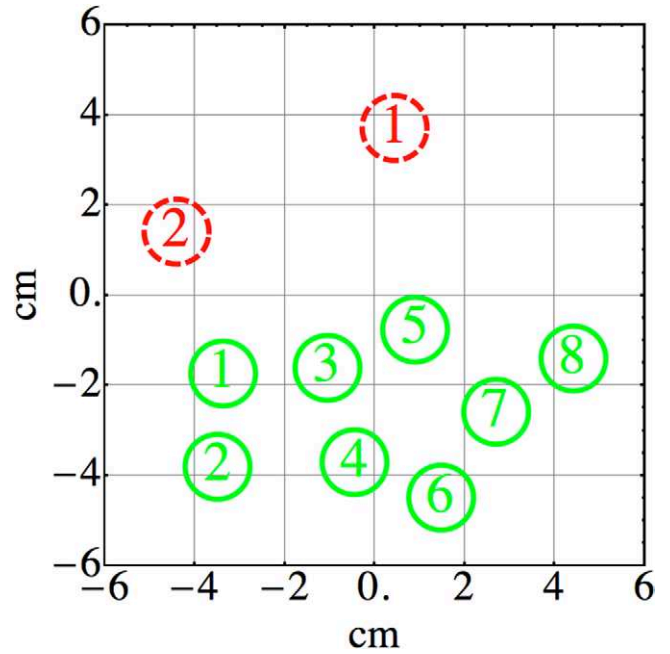ega_R$) and left-hand ($\omega_L$) circularly polarised density cutoffs respectively. The magenta line indicates the plasma frequency cutoff (ω_{pe}). The dotted and continuous orange lines mark the first (ω_{ce}) and second ($2\omega_{ce}$) electron cyclotron harmonics respectively. The dashed grey line indicates the position of the last closed flux surface. The green circles mark the positions of the normal incidence O-mode cutoffs for each of the SAMI frequency channels. The red crosses indicate the locations of the Normal Incidence (NI) right-hand circularly poslarised cutoffs for each of the SAMI frequency channels. The density profile data is from the MAST 130 point Thomson Scattering (TS) system [30].

Figure 3. SAMI array configuration. The layout of the two SAMI emitting (red dashed circles numbered 1–2) and eight receiving antennas (green continuous circles numbered 1–8) in the SAMI array plates as viewed from the plasma facing side.
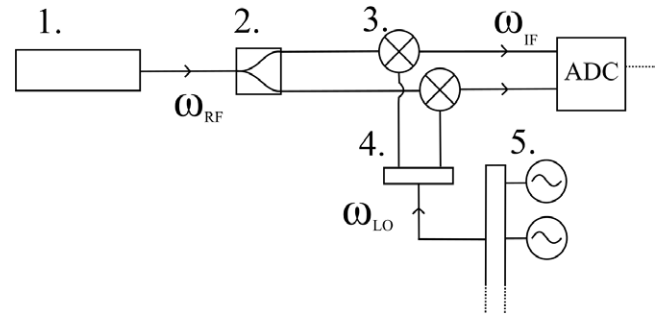
Figure 4. A simplified schematic of the vector heterodyne frequency down-convertor for a single antenna channel. The numbers 1–5 refer to the antenna, hybrid coupler, second harmonic mixers, power splitter and local oscillators respectively.

The backscattered RF signal (ω_{RF}) is received by eight phase sensitive antennas simultaneously. The signal from each antenna (#1 figure 4) is split into *I* and *Q* components by a hybrid coupler (#2 figure 4). The *I* and *Q* components are then downcoverted by second harmonic mixers (#3 figure 4) where the LO signal (ω_{LO}) is generated, via a power splitter (#4 figure 4), by a bank of 5–17.25 GHz dielectric resonance oscillators (#5 figure 4). The IF signal is then digitised by a 14 bit 250 Mega samples per second FPGA-controlled analog to digital convertor (ADC in figure 4).

Upper and lower side band separation is performed using software post shot as outlined in [33]. IF square waves at 10 and 12 MHz from the FPGA are up-converted to the RF frequency using a second harmonic mixer and the LO signal to form the SAMI probing signal. The $2\omega_{LO} + 10$ MHz and $2\omega_{LO} + 12$ MHz signals are launched simultaneouly through active probing antennas 2 and 1 in figure 3 respectively.

The SAMI array is positioned behind a vacuum window made of fused silica. The receiving antennas digitise the backscattered signal along a single polarisation; therefore O and X-mode cannot be separated at present. In section 4 we will discuss the error which this can introduce into our measurements. In future experiments SAMI will be upgraded to dual polarisation antennas which will allow for O and X-mode separation as will be discussed further in section 4.

Figure 5(*a*) shows a poloidal cross section of the installation of SAMI on MAST. The entire vertical extent of the plasma is visible to SAMI apart from the top 20° which is blocked by a poloidal field coil. Figure 5(*b*) shows the response of the system to a point source emitting at 16 GHz.
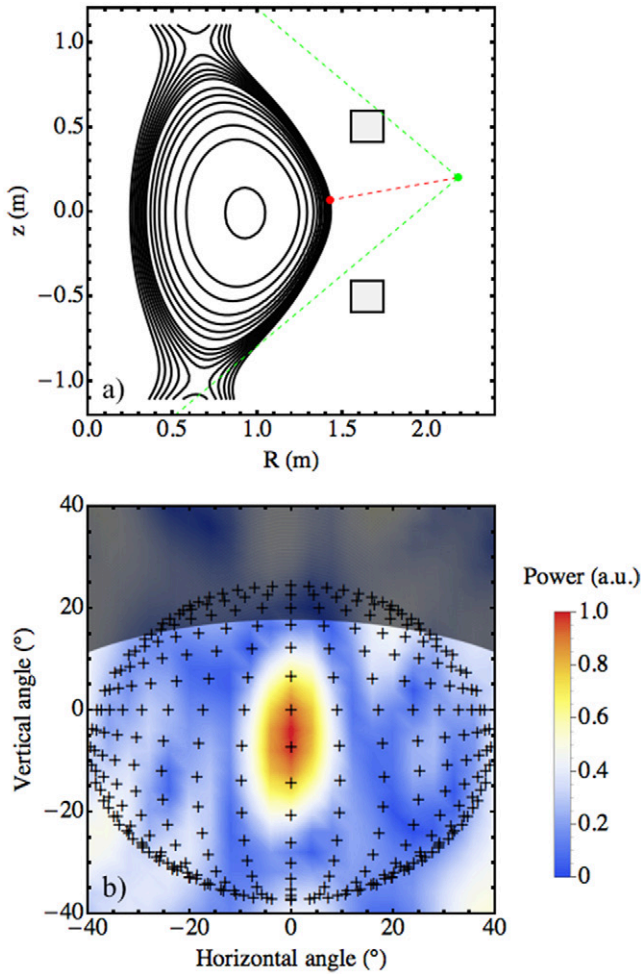
Figure 5. (*a*) Polodial cross-section of the SAMI installation on MAST. The black contours mark the O-mode plasma density cutoff surfaces (constant density along flux surfaces has been assumed) and the upper and lower poloidal field coils are indicated by black squares. The vertical SAMI field of view ($\pm 40°$) is indicated by the green dashed lines. The position of the SAMI array is marked with a green dot. The position of the test source is shown by a red dot. The test source and the SAMI array are connected by a red dashed line. The normal incidence cutoff surfaces were calculated using data from the MAST TS system and EFIT [34, 35]. (*b*) Normalised linear intensity of the SAMI point spread function at 16 GHz in image coordinates. The 3D surface of the normal incidence 16 GHz O-mode cutoff surface is superimposed and indicated by black crosses. The dark region at the top of the plot shows the field of view which is obscured by the upper poloidal field coil.

The power received at the SAMI array is recorded as a function of $\pm 40°$ horizontal and vertical viewing angles. Beam forming has been used to focus the receiving beam at each horizontal and vertical angle in the field of view. Note that although the intensity maximum measured by SAMI is in the correct angular location, the side-lobe power can be up to 50% of the maximum. This high side-lobe level results from SAMI being limited to eight receiving antennas. Future 2D DBS systems could use a greater number of receiving antennas allowing them better directivity as will be discussed further in section 4.

SAMI can also operate in a passive imaging mode, although this is not discussed in this paper. For SAMI passive imaging

experiments and further discussion of the hardware we direct the reader to the relevant papers [31, 33, 36, 37].

2.2. Beam forming

The image inversion algorithm employed on the SAMI active probing data is based on the beam forming technique. Beam forming involves applying a phase shift to each of the antenna channels so that when the phase shifted signals are summed together, constructive interference occurs in a particular direction.

Let us consider a receiving array positioned at the origin of a cartesian coordinate system with its field of view centred along the positive x axis. Let the beam be focused at a generalised point specified by $\boldsymbol{r}$ which is a distance r from the origin and is located at horizontal and vertical angles given by θ and ϕ in SAMI image coordinates respectively. The unit vector, $\hat{\boldsymbol{r}}$, pointing towards $\boldsymbol{r}$ from the origin is given by

$$\hat{\boldsymbol{r}}(\theta, \phi) = \begin{pmatrix} \cos\phi\cos\theta \\ -\cos\phi\sin\theta \\ \sin\phi \end{pmatrix} \tag{2}$$

If the position of the ith antenna in the array is given by $\boldsymbol{x}_i$ and the array is receiving radiation with a wavelength λ, then in order to focus the array at point $\boldsymbol{r}$ the phase shift applied to the ith antenna is given by

$$\psi_i(\theta, \phi) = -\frac{2\pi}{\lambda} |r\hat{\boldsymbol{r}} - \boldsymbol{x}_i| \tag{3}$$

It is intuitive to see that if a point source were placed at $\boldsymbol{r}$ the signal would be received at each of the antennas with a slightly different phase given by equation (3). Therefore applying this phase shift to each antenna signal before summing them together results in constructive interference in the (θ, ϕ) direction. Before being phase shifted and summed together, if one considers the time interval Δt, a Fourier transform is applied to each antenna channel

$$\hat{S}_i^{\text{A}}(\nu) = \int_{\Delta t} S_i^{\text{A}}(t) e^{2\pi j\nu t} \mathrm{d}t \tag{4}$$

where S_i^{A} is the complex signal made up of the I and Q components from the ith antenna ($S_i^{\text{A}} = I_i + jQ_i$) and $j = \sqrt{-1}$. The complex signal from the ith antenna in the frequency domain is denoted by $\hat{S}_i^{\text{A}}$. Applying a Fourier Transform to each antenna channel allows the phase shifts denoted in equation (3) to be applied in the frequency domain. This is computationally advantageous as when conducting active probing SAMI DBS experiments one is typically only interested in a small subset of the available ± 125 MHz IF spectrum; most commonly $\nu_{\text{probe}} \pm 0.2$ MHz where ν_{probe} is the active probing IF frequency. In the frequency domain only the values of interest have to be phase shifted thereby increasing the computational efficiency by a factor of 625 (relative to a time domain phase shift). Let the subset of frequency values included in the receiving beam be denoted by $\Delta\nu$, then the frequency domain synthesised beam signal is given by
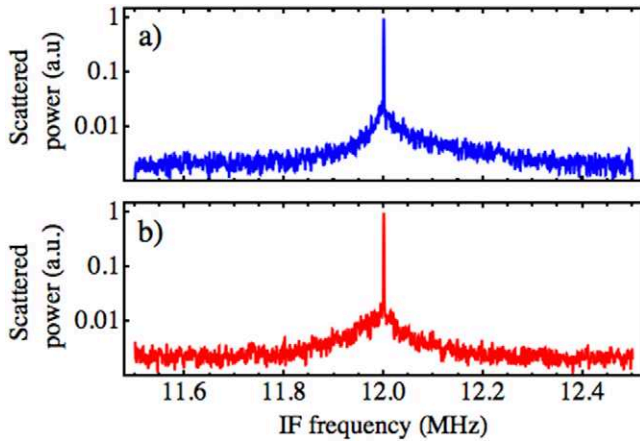
Figure 6. Spectra of the receiving 16 GHz beam around the active probing frequency focused at the points of most blue (*a*) and red-shifted (*b*) power imbalance. Maximum blue and red-shifted power imbalance were observed to be at $(-8°, -12°)$ and $(0°, -28°)$ in image coordinates respectively. Data taken between 290 and 310 ms into MAST shot 27 969.

$$\hat{S}^{\mathrm{B}}(\Delta\nu, \theta, \phi) = \sum_{i=1}^{N} w_i \hat{S}_i^{\mathrm{A}}(\Delta\nu) e^{j\psi_i(\theta, \phi)} \qquad (5)$$

where w_i is a complex calibration factor correcting for amplitude and phase imbalances between antenna channel hardware and the sum is over N antennas. To measure the intensity in the (θ, ϕ) direction within the frequency range $\Delta\nu$, the magnitude of $\hat{S}^{\mathrm{B}}$ is integrated across $\Delta\nu$:

$$I(\Delta\nu, \theta, \phi) = \int_{\Delta\nu} |S^{\mathrm{B}}(\nu; \theta, \phi)|^2 \, \mathrm{d}\nu \qquad (6)$$

By evaluating I over a range of horizontal and vertical viewing angles a 2D map of intensities, such as that shown at the figure 5(*b*), can be plotted.

Erroneously in equation (3) it is assumed that that the location of the source is known. However, in the far field ($r \gg |\boldsymbol{x}_i|$) the phase is not sensitive to r and much more so to the directionality, $\hat{\boldsymbol{r}}$. Therefore, a meticulous value of r is not necessary for accurate image reconstruction. SAMI is sufficiently far away from the plasma in MAST ($\frac{|\boldsymbol{x}_i|}{r} \sim 0.1$) for the far field approximation to hold. In practice r was estimated using the location of the LCFS. If installed on other experiments where $|\boldsymbol{x}_i| \sim r$, it will be critical to make as good an estimate as possible for r using density profile diagnostics and magnetic equilibria reconstructions.

3. Results

3.1. Data analysis techniques

Analysis of SAMI active probing data differs from that used on conventional DBS data. Limited to eight receiving antennas only a *partial* suppression of signal from outside the chosen probing direction is possible. As mentioned in section 1, the back-scattering efficiency is strongly dependent on $K_\perp$. Partial suppression results in the dominant low $K_\perp$ signal affecting all

received spectra. This can make the spectra of received signals difficult to interpret.

Figures 6(*a*) and (*b*) show spectra at 300 ms into MAST shot 27 969 when the 16 GHz beam was focused at the points where the values of blue minus red and red minus blue-shifted power where at their greatest respectively. The red and blue extrema were observed at $(-8°, -12°)$ and $(0°, -28°)$ in image coordinates respectively. On both of these figures there is a large un-shifted power spike at the active probing IF frequency (12 MHz). This is due to reflections off the window and only partially suppressed normal incidence reflections off the plasma.

No Doppler peak is visible in the spectra as obtained during single horn DBS experiments [2, 4–10, 22] due to imperfect side-lobe suppression. In addition, SAMI cannot separate O and X-mode polarisations at present which will increase the number of different $K_\perp$s being sampled, thereby delocalising the scattering location. However, the directional weighting imposed by the phased array does allow a red-blue power imbalance to be measured allowing information to be attained which will be discussed further in section 3.4.

Due to low $K_\perp$ dominance, interference between multiple backscattered signals and both O and X-mode polarisations being present, a quantitative explanation of the observed spectra will require a full-wave treatment; such a study is planned using the cold-plasma full-wave code EMIT-3D [38]. Such a study will aid in turbulent velocity and *k*-spectra measurements through better understanding of observed spectra

The range of $K_\perp$ values which will affect SAMI spectra can be estimated using an analytic formula [4] which takes into account the curvature of the beam and cutoff layer. For a Gaussian probing beam, where the amplitude profile is $E(x) \propto \exp(-x^2/w^2)$ and w is the 1/e beam radius, the range of $K_\perp$ present in the backscattered spectrum is given by

$$\Delta K_\perp = \frac{2\sqrt{2}}{w} \left[1 + \left(\frac{w^2 k_0}{\rho} \right)^2 \right]^{\frac{1}{2}} \qquad (7)$$

where k_0 is the wave vector of the probing beam in vacuum and ρ is the effective curvature radius within the spot $1/\rho = 1/R_{\mathrm{plasma}} + 1/R_{\mathrm{beam}}$. In the Rayleigh region of the beam, $R_{\mathrm{beam}} \to \infty$ so $\rho \to R_{\mathrm{plasma}}$.

The typical radius of curvature for the cutoff layer in a MAST plasma is $R_{\mathrm{plasma}} \sim 1.3$ m. Taking into account the widths of central maxima produces a $\Delta K_\perp$ range of 0.7–2.4 cm^{-1} for 10–34.5 GHz probing.

3.2. k-maps

Figures 7 (*a*) and (*b*) show the distribution of $k_\parallel$ and $k_\perp$ values respectively as a function of probing orientation that are accessible at 16 GHz, 230 ms into MAST shot 27 969 calculated using the beam-tracing code TORBEAM [39]. Doppler backscattering is most efficient when the incident beam is aligned perpendicular to the magnetic field at the scattering location (along $k_\parallel = 0$ in figure 7(*a*)).

We can see from figure 7(*b*) that many values of $K_\perp$ (via equation (1)) can be measured simultaneously using a 2D
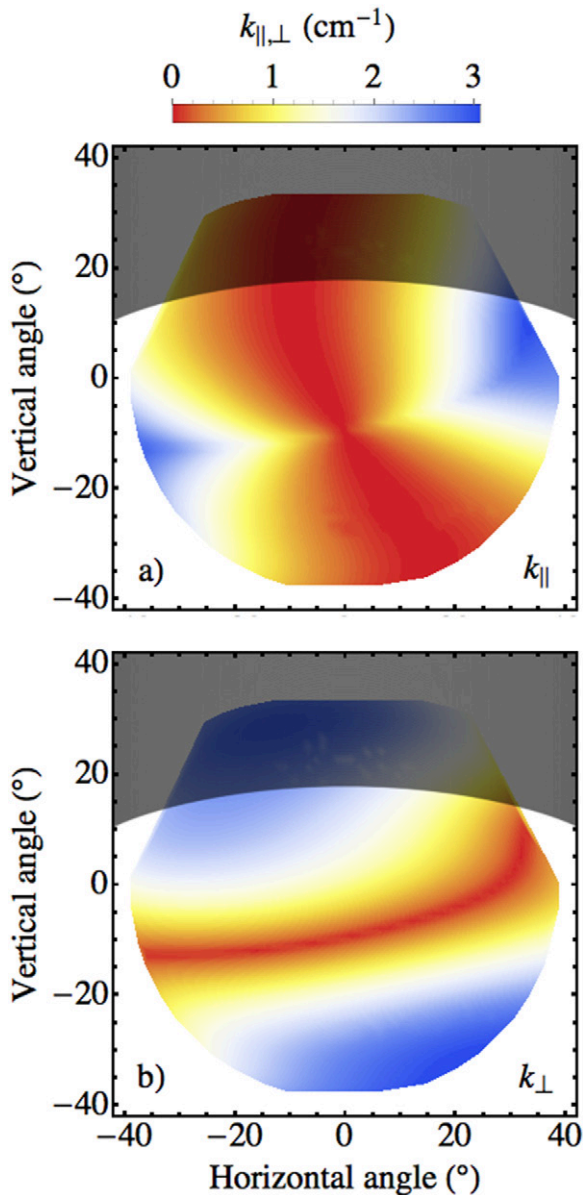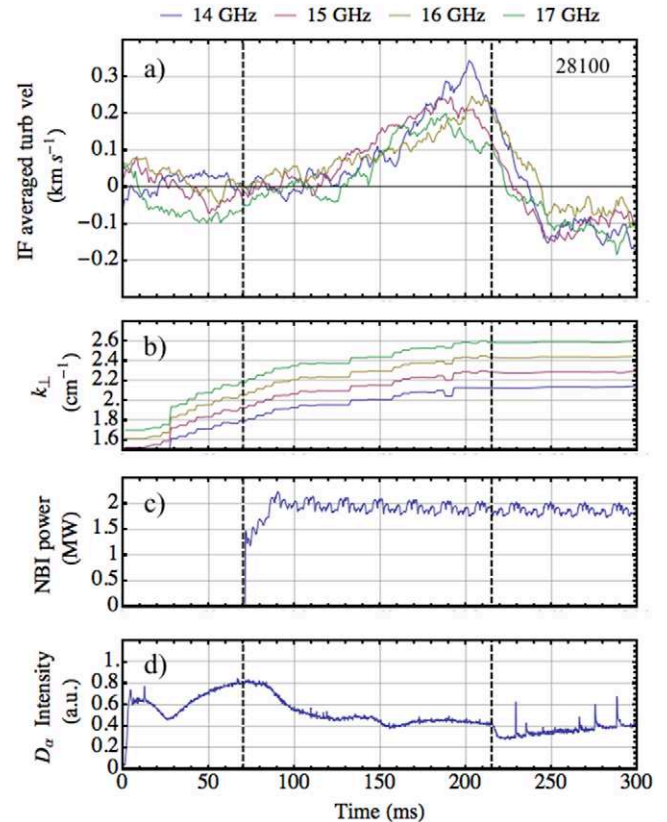
Figure 7. (*a*) and (*b*) show the $k_\parallel$ and $k_\perp$ values of the probing beam at the scattering location for 16 GHz probing as a function of vertical and horizontal viewing angles. Calculated using the beam-tracing code TORBEAM and Thomason Scattering n_e profile data 230 ms into MAST shot 27 969. The dark region at the top of the plots shows the field of view which is obscured by the upper poloidal field coil.

Figure 8. (*a*) 40 ms moving average of IF averaged turbulence propagation velocity for four DBS frequency channels during MAST shot 28 100. Data acquired with the receiving beam focused at ($-20°$, $8°$) and switching in frequency every 200 μs. An IF averaged turbulence velocity was calculated from each frequency step. The black vertical dashed lines at 70 and 215 ms indicate when NBI power is applied and when the plasma enters H-mode respectively. (*b*) The value of the probing beam wavevector at the scattering location for a beam launched in the ($-20°$, $8°$) direction as a function of time as calculated by TORBEAM. (*c*) Co-injected neutral beam power. (*d*) D_α emission.

DBS device although unlike other steerable monostatic DBS systems in its current configuration SAMI has been unable to measure *K*-spectra. This is due to the incomplete directional separation provided by the phased array. Therefore, additional antennas would result in a greatly reduced side-lobe level.

3.3. Initial results

SAMI is a proof of principle diagnostic and DBS experiments have never been attempted using a phased array previously. Limited directional weighting can result in difficult

interpretation of spectra as discussed in section 3.1. However, conducting 2D DBS allows flexibility in the alignment of the probing beam. Figure 8 shows the results from a beam that was aligned with time averaged maximum blue shift during MAST shot 28 100 found at $-20°$ on the horizontal and $8°$ on the vertical. The active probing beam was launched 10 MHz above $2\omega_{LO}$ and the data was digitised on four RF frequency channels: 14, 15, 16 and 17 GHz with a switching time of 200 μs. It is not possible to resolve a discrete Doppler peak in the received spectrum as discussed in section 3.1. The spectra will be a convolution across many probing beam orientations with a directional weighting applied by the phased array. SAMI can still investigate the turbulent velocities of the plasma by looking at the centre of mass of this spectrum. However, this only provides a qualitative comparison with previously observed trends. The centre of mass spectrum will give a gross under estimate of the turbulent velocity at any one point. Forward modelling simulation work is required in order to make a quantitative turbulent velocity comparison to previous charge exchange recombination spectroscopy (CXRS),

beam emission spectroscopy (BES) and conventional DBS experiments.

Figure 8(*a*) shows the 40 ms moving average centre of mass of the turbulence velocity across 10 ± 0.2 MHz in the IF with the central unshifted peak (10 ± 0.01 MHz) notched as a function of time. During these measurements the receiving beam was focused in the $(-20°, 8°)$ direction. The turbulent velocity was calculated from the observed Doppler shift using the value of $k_\perp$ at the scattering location as calculated by TORBEAM (figure 8(*b*)).

A gradual increase in the centre of mass turbulence velocity is observed from 70 ms onwards following 2.5 MW of NBI power being applied by one of MAST's on axis, co-injected, NBI sources (figure 8(*c*)). This rise in observed Doppler shift results from spin-up caused by momentum injection from the NBI system and has been observed during numerous other DBS experiments, for example [2, 10]. Once the plasma enters H-mode at 215 ms (indicated by a decrease in D_α, figure 8(*d*)) there is an abrupt change in the sign of the observed turbulence velocity. A sharp change in the turbulent velocity coinciding with the onset of H-mode has also been measured during previous DBS experiments [2, 10] and results from the edge turbulence velocity being dominated by toroidal fluid velocity during L-mode and diamagnetic velocity in H-mode. The steep pressure gradient that forms in the edge region during H-mode results in a sharp increase of the diamagnetic velocity [2].

Figure 9(*a*) shows the 5 ms moving average of the total Doppler shifted power. The power plotted is the summed power across the IF 10 ± 0.2 MHz where the central unshifted frequency peak is notched (10 ± 0.01 MHz) and the average background noise level is subtracted. The Doppler power steadily increases after the NBI is applied (70–215 ms). This is likely to be caused by an increase in the density (figure 9(*f*)) and the scattering location moving closer to the SAMI array (figure 9(*b*)) and/or an increase in the turbulence amplitude due to an increasing electron temperature gradient at the scattering location (figure 9(*d*)); the electron density gradient stays notably constant during this period (figure 9(*d*)). Temperature and electron density gradients are calculated from Thomson scattering data.

There is a sharp drop in power as the plasma enters H-mode at 215 ms despite the scattering location not changing significantly (figure 9(*b*)). This decrease is caused by the suppression of turbulence in the edge region. The ramp up in power during NBI injection and drop in power as the plasma enters H-mode has been observed in other DBS experiments [3]. In figure 9(*a*) microwave bursts are observed after the plasma enters H-mode as each Edge Localised Mode (ELM) coincides with microwave emission up to four orders of magnitude above thermal [37]. The average background emission is subtracted but this will only nullify the ELM emission if the burst is evenly distributed across the IF.

SAMI has observed trends in turbulence velocity and DBS power which have been observed during previous experiments
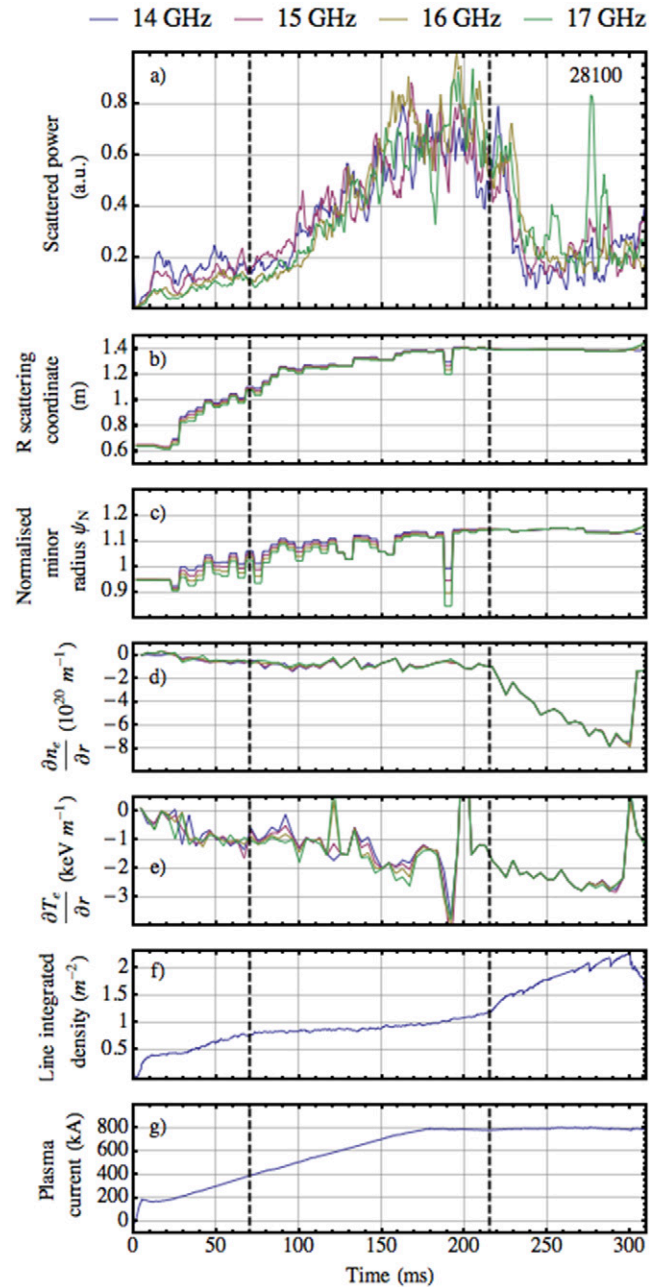
Figure 9. (*a*) 5 ms moving average Doppler shifted power when receiving beam focused at $(-20°, 8°)$. The two black vertical dashed lines at 70 and 215 ms indicate when NBI injection is applied and when the plasma enters H-mode respectively. A value of Doppler shifted power was calculated for each frequency step. (*b*) Major radius (R) scattering location. (*c*) Normalised minor radius of the scattering location. (*d*) The gradient of electron density at the scattering location (derivative with respect to the minor radius). (*e*) The electron Temperature gradient of at the scattering location. (*f*) The line integrated electron density using data form the MAST CO_2 interferometer system. (*g*) Temporal evolution of plasma current.

as demonstrated in figures 8 and 9. Though SAMI has some notable limitations in its current form, the results presented here are encouraging for the future feasibility of 2D DBS systems.
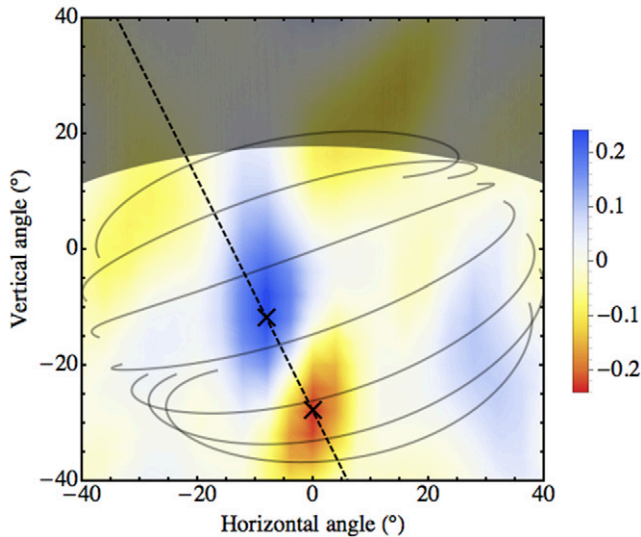
Figure 10. Doppler shifted power difference at 16 GHz during MAST L-mode shot 27 969 at 300 ms. Blue and red indicate more blue than red and more red than blue shifted power respectively. Magnetic field lines on the corresponding normal incidence O-mode cutoff are over-plotted in grey. The maxima and minima in the power deficit between red and blue shifted power are marked with black crosses. The dashed black straight line connects the blue and red maxima. Magnetic field line information and the location of the normal incidence O-mode cutoff surfaces are provided by EFIT and Thomson Scattering respectively.

3.4. Magnetic pitch angle measurements

2D DBS experiments using a phased array could potentially provide a way of measuring the magnetic pitch angle profile with high temporal and spatial resolution.

To form figure 10 the SAMI array was focused, using beam forming, onto each point in an equally spaced 21 by 21 grid spanning ±40° in the horizontal and vertical viewing directions. This was done using data acquired 300 ms into MAST shot 27 969 whilst actively probing the plasma at 16 GHz. For each grid point the spectra of the received beam is analysed.

The red and blue-shifted power was calculated by summing the amplitudes of the signals between 11.8–11.99 MHz and 12.01–12.2 MHz respectively in the IF after subtracting the background passive emission. The total Doppler shifted power was taken as the sum of the red and blue-shifted power. In figure 10 the difference between the blue and red-shifted power is plotted. Net positive and negative regions show where more blue and red-shifted power is present respectively. The colour bar is normalised by dividing the red-blue difference by the total Doppler shifted power. The two regions which show the most red-blue power imbalance are marked with black crosses; the spectra observed at these locations are shown in figures 6(*a*) and (*b*). The black dashed straight line connects the points of maximum blue and red-shifted power imbalance. The magnetic field lines, as calculated from EFIT and Thomson scattering, are over-plotted in grey. Optimum backscattering occurs when the probing beam is perpendicular to the magnetic field lines. Therefore, the orientation of the red and blue maxima allow a pitch angle measurement to
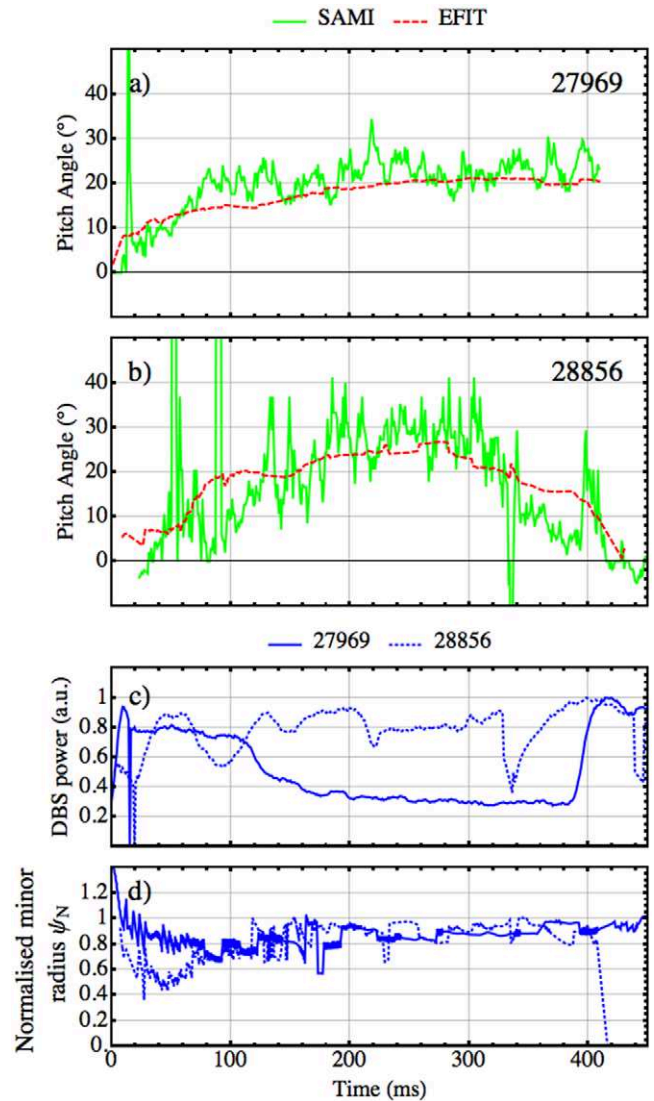
Figure 11. Magnetic pitch angle as measured by SAMI and EFIT at 16 GHz and 10 GHz during MAST shots 27 969 (*a*) and 28 856 (*b*) respectively. The SAMI pitch angle measurement is shown by the solid green line. The magnetic pitch angle as calculated by EFIT is shown by the dashed red line. Each SAMI pitch angle measurement was calculated using 8 ms of data. The EFIT pitch angle was evaluated at the scattering location of a ray launched directly in-between the locations of the red and blue-shifted maxima and minima at each moment in time as calculated by TORBEAM. (*c*) Shows the backscattered power level at the red and blue-shifted Doppler power maxima during shot 27 969 (continuous blue line) and 28 856 (dashed blue line). Note that the power levels for each shot use different normalisations. (*d*) The normalised minor radius (ψ_N) of the scattering location for shots 28 856 and 27 969 as calculated by TORBEAM.

be made. SAMI is the first DBS system to make a pitch angle measurement. This new capability is a direct result of simultaneous 2D imaging made possible by the use of a phased array.

Figures 11(*a*) and (*b*) show the magnetic pitch angle as measured by SAMI (green line) and EFIT (dashed red line) as a function of time for MAST shot numbers 27 969 (fixed frequency 16 GHz) and 28 856 (fixed frequency 10 GHz). A fine grid of 161 by 161 was used within the ±40° viewing

aperture for greater accuracy. The SAMI pitch angle time evolution was calculated using an 8 ms sliding data window. The EFIT pitch angle was calculated at the scattering location of a ray launched along a path directly in-between the locations of maxima and minima in power deficit at each moment in time as calculated by TORBEAM.

The reliability of the SAMI pitch angle measurements relies on there being sufficient backscattered power. Figure 11(*c*) shows the normalised to peak value backscattered power during MAST shots 27 969 and 28 856 where the background passive emission has been subtracted. One can see that the large departure from EFIT by the SAMI pitch at 10 ms during shot 27 969 coincides with a sharp drop in backscattered power. It is also apparent that departures between SAMI and EFIT during shot 28 856 occur between 60–130 ms and 330–350 ms when the DBS power is comparatively low. With a larger database of appropriate data it should be possible derive a relationship between the reliability of the data and back-scattered power.

It is worth noting that the optimum configuration for SAMI to make pitch angle measurements was not known when the data for these shots was taken. Nevertheless, despite being a proof of principle, first of its kind diagnostic, SAMI has made pitch angle measurements which agree well with EFIT considering SAMI's present limitations. The amount of uncertainty in the SAMI and EFIT pitch measurements is left the subject of a future publication. The evolutionary trend in the pitch, as measured by SAMI and EFIT, is in agreement throughout both shots. The fluctuation level in the SAMI pitch angle measurements during shot 28 856 is noticeably higher than during 27 969. This is expected as, being a low frequency 10 GHz shot, more of the probing beam is backscattered in the scrape off layer where the density fluctuation level is high. Though the radial scattering locations are similar in both shots (figure 11(*d*)) the pitch evolution varies due to different plasma current temporal profiles. It is also apparent from figure 11(*d*) that scattering takes place in the edge region consistent with figure 2.

As will be discussed further in section 4 there are numerous ways that SAMI can be upgraded and reconfigured to improve the accuracy of the pitch angle measurements.

4. Further work and discussion

SAMI is a prototype 2D DBS system and after the initial results presented in this paper it is apparent that there are numerous options for further development.

Critical to improving understanding of the SAMI data is better interpretation of the observed spectrum in any one particular direction. The beam formed spectrum results from a convolution of many spectra over the whole field of view with a weighted directionality applied by the phased array. As previously mentioned in section 3.1, accurate *k*-spectra and turbulent velocity measurements rely on a greater understanding of the observed spectra through full wave modelling. Such a study is currently being undertaken.

An improvement to the SAMI system would be to increase the number of receiving antennas. The effective number of pixels in the image is proportional to the square of the number of antennas. Therefore extra antennas would greatly improve the directional weighting that SAMI could apply thereby increasing the accuracy of turbulent velocity measurements by further suppressing backscattered radiation outside the focused beam. Combined with forward modelling, accurate measurements of toroidal rotation velocity could then be compared with CXRS and BES diagnostics. SAMI is currently unable to measure *K*-spectra as measuring the amplitude of a particular *K* requires probing the plasma at a single location. Extra antennas would result in better probing beam localisation improving the accuracy of *K*-spectra measurements. The exact qualitative effect more antennas would have on *K*-spectra measurements requires an involved treatment of antenna optimisation and has many variable factors such as amplitude of the turbulence and plasma geometry and is therefore left as the subject of a future publication.

The arrangement of the antennas in the receiving array could also be changed so that the array was optimised for conducting DBS experiments. For example, the receiving array could be arranged linearly with the antennas aligned with the magnetic pitch angle in order to attain improved spatial directionality along the axis of the array which would allow for increased $K_\perp$ selectivity. The limitation of this technique is that the array would only be optimised for a particular pitch angle and, as is evident in figures 11(*a*) and (*b*), spherical tokamaks have highly variable magnetic pitch.

The SAMI system could also be improved by enabling polarisation separation. All data presented here was obtained using linearly polarised Vivaldi antennas with one polarisation orientation. This means that O and X-mode radiation cannot be separated. It can be seen in figure 2 that the O-mode and X-mode cutoffs are in close proximity during SAMI MAST experiments; therefore interference effects might be significantly affecting the backscattered signal. This is a potential source of error in the turbulent velocity measurements (figure 8(*a*)) and pitch angle measurements (figure 11). In order to attain polarisation separation it is planned to upgrade SAMI's receiving array to dual polarised PCB sinuous antennas [40, 41]. Polarisation separation will then be achieved by fast switching between the two orthogonal polarisations.

When the existing SAMI data set was acquired it was not known how the SAMI system would be optimised for DBS experiments. In figures 11(*a*) and (*b*) pitch angle at one frequency only is plotted. This results from the switching time between frequencies being set too short (10–250 μs). Therefore time integration was not long enough for a pitch angle measurement to be made during switching frequency data acquisitions. Now it is known that longer time integration is required (~10 ms), experiments can be conducted providing pitch angle profiles as a function of time using the existing SAMI system. Effects on pitch angle by NBI and H-mode can then be investigated along with a comparison against Motional Stark Effect (MSE) pitch profiles once a larger, multi-frequency, data set is attained. It is hoped that such a

data set will be acquired after successful installation of SAMI on NSTX-U in late 2016.

5. Conclusion

SAMI has been used to conduct the first ever simultaneous 2D DBS experiments and has explored the feasibility of using a phased array to conduct DBS on fusion plasmas. SAMI has measured phenomena that have been predicted by theory and observed during previous conventional DBS experiments. An increase in the observed turbulence velocity with application of NBI and a sharp transition in velocity during the L-H transition (see figure 8(*a*)) have been observed in MAST. Doppler shifted power has been seen to increase after application of NBI and drops when the plasma enters H-mode (see figure 9(*a*)). As well as reaffirming measurements made by conventional DBS systems, conducting 2D Doppler experiments has allowed the magnetic pitch angle to be measured, a parameter not previously probed by DBS.

Conventional DBS systems have to be aligned at a specific orientation so that their probing beams are perpendicular to the magnetic field at the scattering location. These systems are limited as this orientation will only be optimal for one particular magnetic pitch angle. This problem is exacerbated in spherical tokamaks where the pitch angle may vary considerably (see figures 11(*a*) and (*b*)). As SAMI is always probing in every direction this problem is bypassed and the spatial variability of the backscattering maxima allows a magnetic pitch angle measurement to be made.

Therefore SAMI has shown that it is feasible to conduct DBS experiments using a phased array and that using a 2D system not only allows flexibility in the directionality of the beam, but also allows new parameters to be measured. This has all been accomplished using a prototype system consisting of eight antenna channels and no polarisation separation. Following the discussion in section 4 there are numerous ways which SAMI could be upgraded and improved. In light of the results presented here and the potential routes forward, phased array systems such as SAMI provide an exciting and promising new range of capabilities for DBS diagnostics.

Acknowledgments

References

[1] Holzhauer E. *et al* 1998 *Plasma Phys. Control. Fusion* **40** 1869
[2] Conway G.D. *et al* 2004 *Plasma Phys. Control. Fusion* **46** 951
[3] Hillesheim J.C. *et al* 2009 *Rev. Sci. Instrum.* **80** 083507
[4] Hirsch M. *et al* 2001 *Plasma Phys. Control. Fusion* **43** 1641
[5] Hirsch M. *et al* 2004 *Plasma Phys. Control. Fusion* **46** 593
[6] Zhou C. *et al* 2013 *Rev. Sci. Instrum.* **84** 103511
[7] Weiwen X. *et al* 2008 *Plasma Sci. Technol.* **10** 403
[8] Tokuzawa T. *et al* 2012 *Rev. Sci. Instrum.* **83** 10E322
[9] Pshenichnikov A.A. *et al* 2005 *Plasma Phys. Rep.* **31** 554
[10] Hillesheim J.C. *et al* 2014 *Nucl. Fusion* **55** 073024
[11] Burrell K.H. 1997 *Phys. Plasmas* **4** 1499
[12] Schmitz L. *et al* 2012 *Phys. Rev. Lett.* **108** 155002
[13] Happel T. *et al* 2009 *Rev. Sci. Instrum.* **80** 073502
[14] Hennequin P. *et al* 2004 *Rev. Sci. Instrum.* **75** 3881
[15] Happel T. *et al* 2011 *Proc. of the 11th Int. Reflectometry Workshop* (*Palaiseau, France, 22–24 April 2013*) www.aug.ipp.mpg.de/IRW/IRW11
[16] Hillesheim J.C. *et al* 2010 *Rev. Sci. Instrum.* **81** 10D907
[17] Wang G. *et al* 2013 *Phys. Plasmas* **20** 092501
[18] Conway G.D. *et al* 2005 *Plasma Phys. Control. Fusion* **47** 1165
[19] Huang Z. *et al* 2013 *40th EPS Conf. on Plasma Physics ECA (Espoo, Finland, 1–5 July 2013)* vol 37D P2.175 www.ocs.ciemat.es/EPS2013PAP/html/contrib.html
[20] Sabot R. *et al* 2009 *Nucl. Fusion* **49** 085033
[21] Gurchenko A.D. *et al* 2013 *Plasma Phys. Control. Fusion* **55** 85017
[22] Bulanin V.V. *et al* 2011 *Tech. Phys. Lett.* **37** 340
[23] Hennequin P. 2006 *C. R. Phys.* **7** 670
[24] Gusakov E.Z. *et al* 2004 *Plasma Phys. Control. Fusion* **46** 1143
[25] Blanco E. *et al* 2006 *Plasma Phys. Control. Fusion* **48** 699
[26] Ida K. 1998 *Plasma Phys. Control. Fusion* **40** 1429
[27] Gusakov E.Z. *et al* 2005 *Plasma Phys. Control. Fusion* **47** 959
[28] Gibson P.J. 1979 *Proc. of the 9th European Microwave Conf.* (*Brighton, UK, 17–20 September 1979*) pp 101–5 http://ieeexplore.ieee.org/xpl/articleDetails.jsp?arnumber=4131323
[29] Langley J.D.S. *et al* 1996 *IEE Proc. Microw. Antennas Propag.* **143** 97
[30] Scannell R. *et al* 2010 *Rev. Sci. Instrum.* **81** 10D520
[31] Freethy S.J. 2012 Synthetic aperture imaging of B-X-O mode conversion *PhD Thesis* University of York http://etheses.whiterose.ac.uk/2352/
[32] Freethy S.J. *et al* 2012 *IEEE Trans. Antennas Propag.* **60** 5442
[33] Shevchenko V.F. *et al* 2012 *J. Instrum.* **7** 10016
[34] Lao L.L. *et al* 1985 *Nucl. Fusion* **25** 1611
[35] Appel L.C. *et al* 2006 *33rd EPS Conf. on Plasma Physics ECA (Rome, Italy, 19–23 June 2006)* vol 30I P2.160 http://epsppd.epfl.ch/Roma/start.htm
[36] Freethy S.J. *et al* 2013 *Plasma Phys. Control. Fusion* **55** 124010
[37] Freethy S.J. *et al* 2015 *Phys. Rev. Lett.* **114** 125004
[38] Williams T.R.N. *et al* 2014 *Plasma Phys. Control. Fusion* **56** 075010
[39] Poli E. *et al* 2001 *Comput. Phys. Commun.* **136** 90
[40] O'Brient R.C. 2010 A log-periodic, focal-plane architecture for cosmic microwave background polarimetry *PhD Thesis* University of California Berkeley
[41] Saini K.S. 1996 National radio as- tronomy observatory green bank, west virgina electronic division internal memo www.gb.nrao.edu/electronics/edir/edir301.pdf